Scaling of Impact on Glass-Polyester Laminated Plates

L.S. Sutherland & C. Guedes Soares
Unit of Marine Technology and Engineering, Technical University of Lisbon,
Instituto Superior Técnico, Av. Rovisco Pais, 1049-001 Lisbon, Portugal

ABSTRACT: A dimensional analysis approach was used to develop scaling laws for impact on marine composite materials. An experimental study was performed to verify these relationships for the transverse impact of a hemispherical ended impactor on fully-clamped circular hand laid-up glass-polyester plates at three different scales. A simplified model, assuming a homogenous and isotropic material, scaled the impact responses very well for the elastic response. However, 'size effects' were observed, especially for the damaged response, but further work is required to fully explain the mechanisms behind these effects.

1 INTRODUCTION

Composite materials are susceptible to impact damage, and the problem has received much attention in the literature (Abrate 1988). However, the great majority of the existing work concerns high fibre volume-fraction, pre-preg carbon-epoxy autoclaved laminates as used in the aerospace industry. This study concerns much more variable hand laid-up lower priced, low fibre-content glass-polyester composites as commonly used in the marine industry.
Impact on composites is a complex problem largely because large deflections, shear deflections, membrane effects and non-linear contact behaviour are significant, and because it is a dynamic event involving numerous and interacting damage modes. Further, the impact response and damage modes are sensitive both to many material and many impact parameters.

Hence, confidence in theoretical predictions is not high, especially concerning damage, and so experimental validation of the design process is often necessary. Full-scale testing may not be feasible, and is certainly expensive, and hence scale model testing is attractive.

However, there are scaling issues; unforeseen phenomena or differences in behaviour that lead to errors in full-scale prototype predictions obtained from model tests must be avoided or at least allowed for. Such prediction errors are referred to as 'size-' or 'scale-effects'.

Considerable work has also been carried out in the area of size-effects in composites testing, with a general consensus that these effects are significant, but that there is no one single phenomenon because of the various failure mechanisms involved (Wisnom 1999).

Work specifically concerning the scaling of the impact on composites is much scarcer, however, and a review of these studies may be found in Sutherland & Guedes Soares (2007). In summary, the use of scaling laws has been successful for the elastic response of high volume-fraction pre-preg carbon laminates, but damage size-effects were significant.

The aim of the present work is to investigate experimentally the impact scaling of low fibre-volume hand-produced glass-polyester laminates using a scaled model approach.

2 SCALING THEORY

In this section scaling rules for the central, transverse impact of a fully clamped composite plate with a hemispherical ended impactor 'head' are developed using dimensional analysis techniques and the theory of models (David & Nolle 1982, Langhaar 1951, Taylor 1974, Ambur et al. 2005).

Firstly it is necessary to decide which response is to be scaled. In this paper this *test variable* will be the central transverse displacement, *w(t)*. In order to simplify what is an extremely complex event, the impact behaviour of the composite is assumed to be sufficiently approximated by that of a homogenous and isotropic material.

Making a list of all of the variables thought to be relevant:

Specimen thickness	h
Specimen Radius	R
Specimen Poisson Ratio	υ
Specimen Young's Modulus	E

Specimen Density	ρ
Impactor Head Radius	R_i
Impactor Mass	m_i
Impactor Poisson Ratio	υ_i
Impactor Young's Modulus	E_i
Impactor Density	ρ_i
Incident Velocity	V_i

Using mass (M), length (L) and time (T) as the primary quantities and applying the Buckingham Pi theorem gives the 10 required (i.e. 13 variables minus 3 primary quantities) Pi terms given below. This particular set is not the only possible one, but has been selected because most of the terms have fairly straightforward physical interpretations.

Test Parameter: $\Pi_1 = w/h$, (1)

Design Parameters:

'Geometric' $\Pi_2 = R/h$, $\Pi_3 = R_i/h$, (2)

'Material Property' $\Pi_4 = \upsilon$, $\Pi_5 = \upsilon_i$, $\Pi_6 = \rho/\rho_i$, $\Pi_7 = E_i/E$ (3)

'Impact Event' $\Pi_8 = V_i^2 \rho_i / E$, $\Pi_9 = m_i / h^3 \rho_i$, $\Pi_{10} = tV_i/h$ (4)

Now the model needs to be designed to ensure that the test parameter (Π_1) is the same for model and prototype. The theory of models shows that to do this it is necessary to scale all of the relevant variables between model and prototype so that all the design parameters (Π_{2-10}) are also the same for model and prototype. If this is achieved (and this is not always physically possible) then the model is said to show complete similarity to the prototype. Defining the scaling factor, λ, of a variable as the ratio of its value for the prototype to that for the model, for example, for displacement:

$$\lambda_w = w_p / w_m \quad (5)$$

where subscripts *p* and *m* refer to prototype and model respectively.

Hence, extending this definition to the Pi terms gives the following relationship for complete similarity:

$$\lambda_\Pi = 1 \text{ for all } \Pi \quad (6)$$

where, if $\Pi = f(x_1 \ldots x_j)$, then $\lambda_\Pi = f(\lambda_{x1} \ldots \lambda_{xj})$.

Constructing a model that is a geometrically scaled version (by a scaling factor of *s*) of the prototype will ensure that both $\lambda_{\Pi 2}$ and $\lambda_{\Pi 3}$ are unity:

$$\text{i.e. } \lambda_h = \lambda_R = \lambda_{Ri} = s \quad (7)$$

Using the same materials for the model as for the prototype, and using the same material for the impactor in both cases, will ensure that all of the material property scaling parameter factors ($\lambda_{\Pi 4}$ to $\lambda_{\Pi 7}$) are also unity:

$$\text{i.e. } \lambda_\nu = \lambda_{\nu i} = \lambda_\rho = \lambda_{\rho i} = \lambda_E = \lambda_{Ei} = 1 \quad (8)$$

Now it only remains to ensure that the impact event itself is properly scaled, and to do this the scaling factors of the remaining Pi terms must also be unity:

$$\lambda_{\Pi 8} = \lambda_{Vi}^2 \lambda_{\rho i} / \lambda_E = 1, \text{ i.e. } \lambda_{Vi} = 1 \quad (9)$$

That is, the impact velocity (and hence the drop height) should be the same at model and prototype scales.

$$\lambda_{\Pi 9} = \lambda_{mi} / \lambda_h^3 \lambda_{\rho i} = 1, \text{ i.e. } \lambda_{mi} = s^3 \quad (10)$$

That is, the prototype impact mass should be s^3 times that of the model.

$$\lambda_{\Pi 10} = \lambda_t \lambda_{Vi} / \lambda_h = 1, \text{ i.e. } \lambda_t = s \quad (11)$$

Since it is not possible to scale time this means that something that takes 1 second in the model will take *s* seconds in the prototype.

In summary, when target and impactor head are geometrically scaled as *s*, the same materials are used for model and prototype throughout, and the impact mass is scaled as s^3 and dropped from the same drop height for model and prototype, then we have complete similarity and the central displacement response should also scaled geometrically as *s*.

$$\text{i.e. } \lambda_w = w_p / w_m = s \quad (12)$$

It was already noted that time is also scaled by s, so the impact duration of the prototype would be expected to be s times that of the model, and now we will consider how the other commonly used impact responses scale in our model.

Adding the variable impact force, *P*, to the initial list and applying Buckingham Pi theory gives an additional Pi term:

$$\Pi_{11} = P/h^2 E, \text{ i.e. } \lambda_P = s^2 \quad (13)$$

That is, the prototype impact force will be s^2 times that in the model.

Similarly, for the absorbed energy, *AE*:

$$\Pi_{12} = AE/h^3 E, \text{ i.e. } \lambda_{AE} = s^3 \quad (14)$$

That is, the prototype absorbed energy will be s^3 times that in the model.

The same method could also be used for the incident energy, *IE*;

$$\Pi_{13} = IE/h^3 E, \text{ i.e. } \lambda_{IE} = s^3 \quad (15)$$

It should be noted that the scaling model used here is simplified. Many aspects, such as the non-homogeneous and non-isotropic nature of the composite materials, the effect of damage, contact stiffness and possible strain-rate effects (c.f. $\lambda_t = s$) have not been included in the analysis. If any of these aspects have a significant effect on one or more of the responses then the lack of this effect in this simple analysis could lead to a 'distorted model'. This would produce deviations from the predictions of the analysis, which are often termed 'size-' or 'scale-effects'.

Here, the scaling analysis of the central impact of a fully clamped composite plate described above is verified through an experimental study. A series of tests are carried out at the model scale (i.e. $s = 1$) and these results compared with equivalent tests at two larger prototype scales ($s = 2$, and $s = 3$).

3 EXPERIMENTAL DETAILS

One metre square panels of orthotropic polyester resin reinforced with E-glass were laminated by hand. Two series of panels were fabricated; one using a $500gm^{-2}$ woven roving (WR) reinforcement and one using $450gm^{-2}$ chopped strand mat (CSM). Fibre mass-fractions were 0.5 (volume fraction 0.35) and 0.3 (volume fraction 0.2) for WR and CSM laminates respectively. Square specimens were cut from the panels using a diamond-surrounded circular saw, and thickness measurements taken at four points on each. As explained in section 2, specimens were geometrically scaled, and details are given in Table 1.

	s	No. Plies	Thick (mm)	Clamp ∅ (mm)	Impact Mass (kg)	Head ∅ (mm)
WR	1	5	3.06	100	3.103	10
∅ = 32	2	10	6.14	200	24.92	20
Thick	3	15	9.44	300	84.22	30
WR	1	10	6.29	100	3.103	10
∅ = 16	2	20	12.12	200	24.92	20
Thick	3	30	18.30	300	84.22	30
CSM	1	5	4.63	100	3.103	10
∅ = 22	2	10	8.84	200	24.92	20
Thick	3	15	14.36	300	84.22	30
CSM	1	10	8.67	100	3.103	10
∅ = 11	2	20	18.54	200	24.92	20
Thick						

Table 1: Specimen and Test Details

A fully instrumented falling weight machine (Rosand IFW5) was used for the impact testing. A light, hemispherical-ended cylindrical 'impactor head' attached to a much larger, variable mass was dropped from a known, variable height between guide rails onto the target. As per section 2, the impactor heads were also geometrically scaled and the impact mass scaled as s^3 (see Table 1).

The horizontally supported specimens were fully clamped between thick steel annular plates to give the scaled specimen diameters. The thickness of the different clamping plates was also scaled geometrically.

A load cell between the impact mass and head gave the variation of impact force with time. An optical gate measured the incident velocity, and hence the impactor displacement and velocity and the energy it imparts could be calculated from the force-time data by successive numerical integrations. A pneumatic catching device, triggered by the return through the optical gate, prevented further rebound impacts. This device was not robust enough to be used for the largest impact mass (s = 3), and that rebounds occurred for this largest scale should be noted when considering the damage sustained by these specimens. However, the corresponding impact responses were not affected since they were measured only during the initial impact.

Since the impactor is assumed to remain in contact with the specimen throughout the impact event, the impactor displacement is used to give the displacement and velocity of the impacted face of the specimen. By assuming that frictional and heating effects are negligible, the energy imparted by the indenter is that absorbed by the specimen. Thus, this energy value at the end of the test is that irreversibly absorbed by the specimen.

The force data was post-processed with a low-pass discrete 2nd order Butterworth filter to remove noise from the signal. Cut-off frequencies were selected to ensure no loss of pertinent features, and were also scaled as $1/s$ (as closely as possible) since time scales as s (Table 1). All data presented here is filtered for clarity, but the entire analysis was also duplicated using the raw data to confirm that the results were not affected by data filtering.

Each row in Table 1 corresponds to a series of tests on nominally identical specimens performed at a range of increasing incident velocities and hence energies. After testing, any damage was observed and noted, and the projected area of internal delamination(s) could be measured using strong back-lighting since the materials considered are translucent.

4 RESULTS

The damage progression seen followed that detailed in previous work (Sutherland & Guedes Soares 2005a, 2006). Circular internal delamination occurred at very low incident energy for all tests. At higher energies, these delaminations grew and then fibre damage occurred. The thinner specimens tended to give 'back-face fibre damage' as large global deflections gave high strains. The thicker specimens tended to first give permanent indent damage on the 'front' or impacted face that then developed into 'front-face fibre damage'. In both cases, once the initial damage became more severe with increasing energy, fibre damage could occur on the other face, leading to penetration, and finally perforation. 'Fibre failure' of the WR laminates consisted of breakage of the continuous fibres, whereas

for CSM laminates 'pull-out' of the short discontinuous fibres occurred.

The force-displacement behaviour reflected the damage progression. The thicker WR and CSM response was as previously seen (Sutherland & Guedes Soares 2005a, 2006); a bi-linear force-displacement response with a sudden reduction in stiffness as delamination occurred, and at higher impact energies a drop in force or an inflection due to fibre damage was evident.

The thinner WR tests for the test scales s = 1 and 2 exhibited the increasing stiffness and decreasing impact duration associated with membrane effects (Sutherland & Guedes Soares 2005a, 2006), but these were not present for the larger, s = 3 scale (see Section 5.3). Although delamination of the thinner WR specimens also occurred, no corresponding drop in stiffness was discernable (Sutherland & Guedes Soares 2005a, 2006).

The thinner CSM response also showed membrane stiffening effects for s = 1 and 2, but these were weaker than for the thinner WR. Again these membrane effects were not present for the larger, s = 3 tests. However, for the thinner CSM specimens, a sudden drop in stiffness accompanied delamination.

The test results may be most clearly and concisely summarised graphically; the test variable of central deflection and the other impact responses are plotted in Figure 1 to Figure 5. The appropriate scaling factors obtained in Section 2 are used to directly compare the responses at different scales. Section 2 also showed that scaling equivalence is obtained when the same incident velocity is used at each scale, and hence these responses are plotted against incident velocity. This also allows valid comparisons to be made when slight differences between nominal and obtained incident velocities occurred.

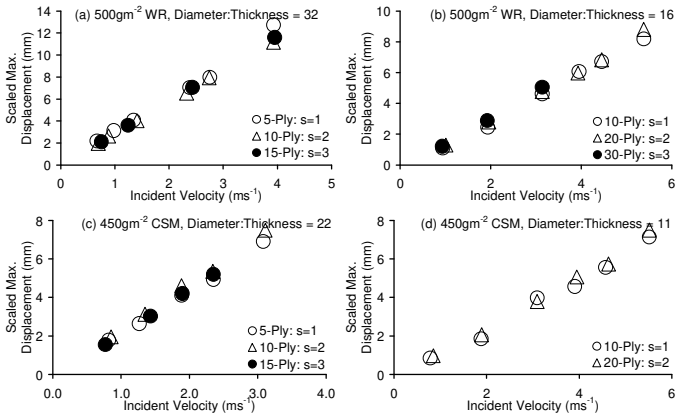

Figure 1: Scaled Maximum Displacement Results (Scale factor s)

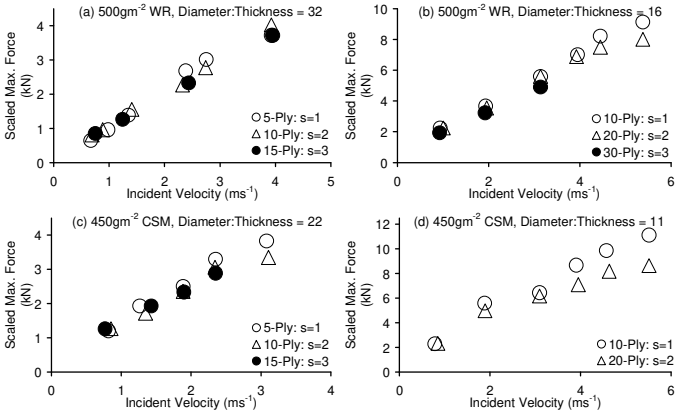

Figure 2: Scaled Maximum Force Results (Scale factor s^2)

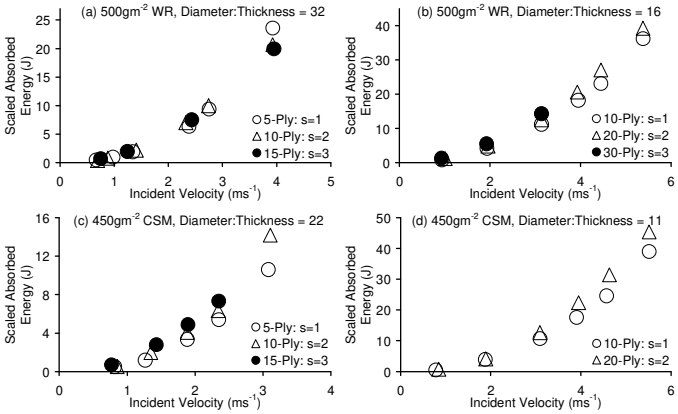

Figure 3: Scaled (Irreversibly) Absorbed Energy Results (Scale factor s^3)

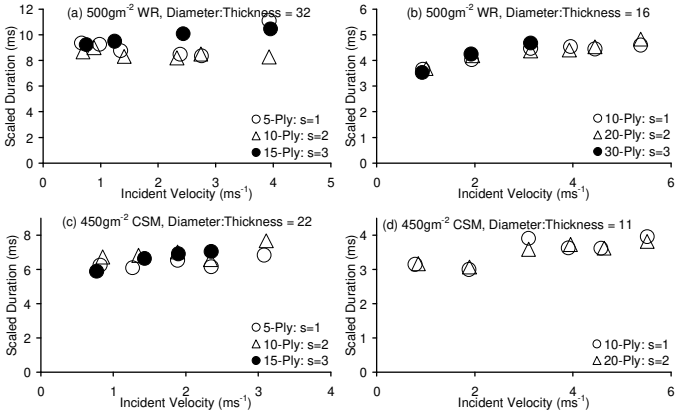

Figure 4: Scaled Impact Duration Results (Scale factor s)

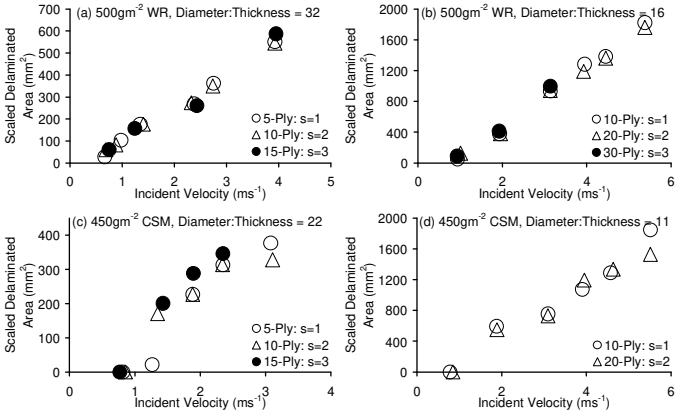

Figure 5: Scaled Delaminated Projected Area Results (Scale factor s^2)

5 DISCUSSION

Although it was assumed that the composite material is homogeneous and isotropic, the scaling approach used here produced very accurate results. Figure 1 shows quite clearly that the central deflection has been scaled extremely successfully. Figure 2 to Figure 5 show that the approach also scales very well the impact responses of maximum force, absorbed energy, impact duration and even projected delaminated area.

However, there are some deviations from the analysis (i.e. 'size-' or 'scale effects') and these are discussed below.

5.1 *Fibre Damage*

Figure 2(b and d) show that at higher incident velocities the maximum force is lower for larger scale. This is accompanied by the higher absorbed energies for the larger scale at higher incident velocities shown in Figure 3(b and d). This behaviour is due to the observation that fibre damage became more severe and occurred at lower incident velocities with increasing scale. The observed damage modes have been presented in Figure 6, where the fraction of incident energy that is irreversibly absorbed is plotted against incident velocity

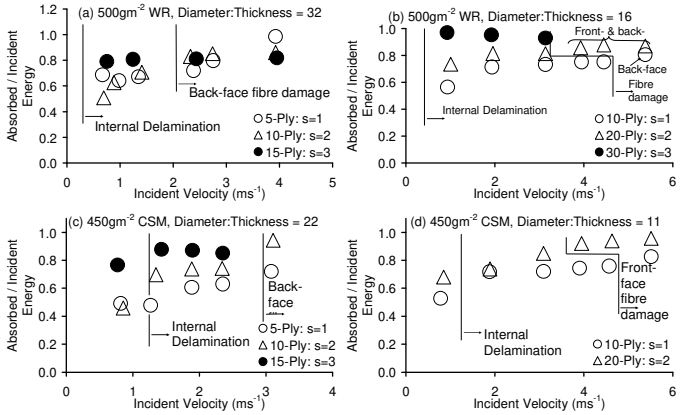

Figure 6: Absorbed to Incident Energy Ratio Results

The thicker WR and CSM specimens show clearly a fibre damage 'size effect'; damage is observed at a lower incident velocity for $s = 2$ than for $s = 1$. It is not clear what is responsible for this size effect. The complex damage modes that occur mean that this is almost certainly not straightforward, especially since there is evidence that failure modes may themselves vary with scale (Figure 6(b)).

Furthermore, Figure 7 shows the points (in terms of force-displacement) at which fibre damage initiated during the relevant tests. This figure clearly shows this onset of fibre damage size effect not only for thicker specimens, but also for thinner specimens.

Figure 7 also shows that for the thinner WR specimens an increase in impact velocity delays fibre damage, i.e. strain-rate is influential in some way. This effect is large considering the very small changes in strain rate involved and hence the mechanism may well be more complex than that of the (relatively) straightforward strain-rate dependency of the strength of composites (Zhou & Davies 1995, Hancox & Mayer 1993).

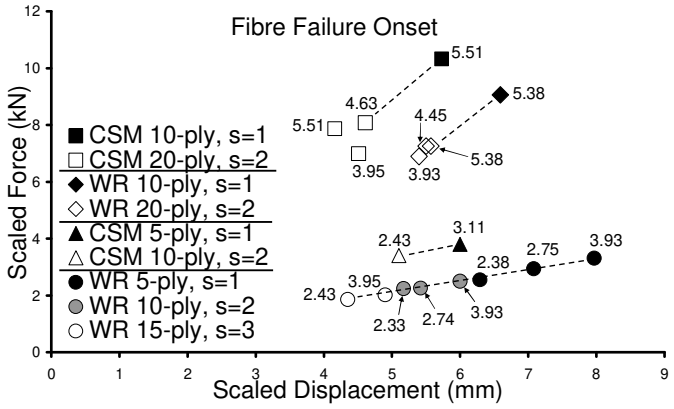

Figure 7: First Fibre Failures (Labels are Incident Velocities in ms^{-1})

It is also possible that the observed 'size effect' could be inextricably linked with the 'strain rate' effect, since for these tests as scale is increased the strain rate must decrease (i.e. $\lambda_t = s$).

Hence, it is only reasonable to conclude that 'size' and 'strain rate' effects on initial fibre damage have been identified, but that further studies, specifically designed to investigate these effects, are required to fully explore the mechanisms responsible.

5.2 *Absorbed Energy*

Closer inspection of Figure 3 indicates that a weaker trend of increasing absorbed energy with scale is also present at lower incident velocities before fibre damage occurs. In Figure 6 the fraction of incident energy irreversibly absorbed is plotted to show more clearly that this absorbed energy 'size effect' is significant for all except the thinner WR specimens.

Although there is no fibre damage in this case, it is probable that one or more of the other damage modes is also more severe at larger scales.

First indentation damage is considered. The scaled displacement at which the impact force falls to zero is assumed to be the point at which the impactor head leaves the specimen surface. For the thicker WR & CSM laminates these values increased with scale, indicating that there is relatively more permanent indentation for large scales.

Previous indentation work (Sutherland & Guedes Soares 2005b) has found the contact behaviour of these laminates to follow a Hertzian law (Johnson 1985) at lower contact forces, followed by a change to linear behaviour at a critical load, P_{crit} as significant contact damage occurs.

For the Hertzian behaviour,

$$P = n\alpha^{3/2} \tag{16}$$

where the contact stiffness, $n = \frac{4E^* \sqrt{R_i}}{3}$, $\frac{1}{E^*} = \frac{1-\nu_i^2}{E_i} + \frac{1-\nu^2}{E}$, and α is the indentation.

$$\text{Hence, } \alpha = \left(\frac{3P}{4E^* \sqrt{R_i}} \right)^{2/3} \tag{17}$$

$$\text{i.e. } \lambda_\alpha = s \tag{18}$$

That is the Hertzian indentation should scale geometrically, indicating no size effect. However, the previous work (Sutherland & Guedes Soares 2005b) showed the contact stiffness *n* not to be proportional to $\sqrt{R_i}$ as expected, and this departure from the theory could be a possible source of the absorbed energy size effect.

The following expression was developed for P_{crit}

$$P_{crit} = \sqrt{\frac{6ILSS^3\pi^3h^3R_i}{E}} \tag{19}$$

$$\text{i.e. } \lambda_{Pcrit} = s^2 \tag{20}$$

This suggests that there should also be no size effect due to the transition to linear contact behaviour.

The controlling mechanisms of the linear contact stiffness behaviour are not yet understood, and hence it is not possible to state whether this is responsible for any size effects. Similarly, little is known about the forms of the indentation 'unloading curves' (the response as the load falls), and so again this behaviour may or may not contribute to the observed absorbed energy size effect.

Even slight differences in the material itself could also affect the indentation behaviour between scales. For example, the degree of (hand) consolidation of the top layers could change with the number of unstable wet plies under them. Also, perhaps the fact that the reinforcement is not scaled could lead to differences in indent behaviour, for example due to the different relative sizes at each scale of the impactor head and the weave or chopped fibre dimensions.

Hence, indentation damage could contribute to the absorbed energy size effect, but the mechanisms are complex and not yet fully understood. However, Nettles et al. (1999) found that dent depths did not scale, and hence this suggests that contact damage could be at least partly responsible for this absorbed energy effect.

Next, delamination is considered as another potential mechanism. The delaminated areas scale very well suggesting that this failure mode does not absorb relatively more energy at larger scales. However, these values are only projected areas, the exact nature of the delaminations is more complex, and so it is still possible that delamination contributes in some way to the absorbed energy size effect.

Finally perhaps other unconsidered damage, or other, mechanisms are responsible. Previous work (Sutherland & Guedes Soares 2006) found that even when no visible damage occurred, most of the incident energy was irreversibly absorbed. It is not yet known if this energy is absorbed by unseen damage such as matrix cracking, or by other mechanisms such as visco-elastic damping or friction. Hence, such mechanisms could also be fully or partly responsible for this absorbed energy effect, but more information is required.

Hence, given the number and complexity of possible explanations, it may only be concluded that further study is required before it is possible to clarify the observed scale dependency of absorbed energy.

5.3 *Impact Duration*

In Figure 4(a) the scaled impact durations of the WR *s* = 3 (15-ply) specimens increase with incident velocity, whilst those of the two smaller scales decrease due to membrane stiffening effects as noted in Section 4. A similar, but weaker trend is also visible in Figure 4(c).

In order to further explore this, the bending, shear and membrane stiffness' k_b, k_s and k_m are introduced into the dimensional analysis;

$$\Pi_{14} = k_b/hE \text{ , i.e. } \lambda_{kb} = s \tag{21}$$

$$\Pi_{15} = k_s/hE \text{ , i.e. } \lambda_{ks} = s \tag{22}$$

$$\Pi_{16} = k_m h/E \text{ , i.e. } \lambda_{km} = 1/s \tag{23}$$

This might appear to suggest that membrane effects should become less important with increasing scale.

$$\text{However, } P = P_m + P_{bs} = k_{bs}w + k_m w^3 \tag{24}$$

$$\text{where } k_{bs} = \frac{k_b k_s}{k_b + k_s} \text{ giving } \lambda_{kbs} = s \text{ , } \tag{25}$$

Hence, the 'stiffness' (in terms of the variation of force with displacement) scales as s^2 for both bending/shear and membrane stretching.

$$\text{i.e. } \lambda_{Pbs} = \lambda_{Pm} = s^2 \tag{26}$$

That is, the scaled force-displacement plots and the relative effects of membrane and bending/shear on impact duration should not change with scale.

Looking elsewhere, a plausible explanation is that despite the efforts to scale the clamping system the boundary conditions at the largest scale were not exactly equivalent to those at the smaller scales. Greater slippage of specimen between the clamps could be responsible, but through-bolting should have prevented this, and no damage to the holes in the larger specimens indicated that this had in fact

occurred. However, it was not practicable to exactly scale the entire clamping/support set-up and so relatively larger clamping/support deflections due to the much higher membrane forces at the largest scale are also still possible explanations.

Again this effect requires further investigation, but initial findings indicate that the exact scaling of the boundary conditions is extremely important.

6 CONCLUSIONS

A dimensional analysis approach was used to develop scaling laws for impact on marine composite materials. An experimental study was performed to verify these relationships for the transverse impact of a hemispherical ended impactor on fully clamped circular plates at three different scales.

Although the model was a simplified one, the tests showed that it scaled the impact responses extremely well for the elastic response.

However, deviations from the predictions with scale, or 'size effects' were observed:

- The onset of fibre failure was found to be at a relatively lower load and displacement for larger scale specimens.
- For thinner woven roving specimens a higher strain rate also resulted in an earlier fibre failure.
- Relatively more energy was irreversibly absorbed for larger specimens even before fibre damage occurred.
- Membrane stiffening effects were weakest at the largest scale.

The mechanisms behind these effects have been discussed, and postulations made on the bases of the observations made, but further work is required, especially to investigate the scaling of fibre failure and how this relates to penetration and finally perforation.

7 ACKNOWLEDGEMENTS

This work has been performed within the project "MARSTRUCT - Network of Excellence on Marine Structures" (http://www.mar.ist.utl.pt/marstruct/) and has been partially funded by the European Union through the Growth programme under contract TNE3-CT-2003-506141. The first author is financed by the Portuguese Foundation of Science and Technology under the contract number SFRH/BPD/20547/2004.

8 REFERENCES

Abrate, S. 1998. *Impact on Composite Structures*. Cambridge: Cambridge University Press.

Ambur, D.R., Prasad, C.B., Rose, C.A., Feraboli, P. & Jackson, W.C. 2005. Scaling the nonlinear impact response of flat and curved anisotropic composite plates. In *Proceedings of 46th AIAA/ASME/ASCE/AHS/ASC Structures, Dynamics and Materials Conference, Austin, TX*.

David, F.W. & Nolle, H. 1982. *Experimental modelling in engineering*. London: Butterworths.

Hancox, N.L. & Mayer, R.M. 1993.*Design Data for Reinforced Plastics*. London: Chapman and Hall.

Johnson, K.L. 1985. *Contact mechanics*. Cambridge: Cambridge University Press.

Langhaar, H.L. 1951. *Dimensional analysis and theory of models*. New York: Wiley.

Nettles, A.T., Douglas, M.J. & Estes, E.E. 1999. Scaling effects in carbon/epoxy laminates under transverse quasi-static loading. *NASA Technical Memorandum NASA/TM-1999-209103*.

Sutherland, L.S. & Guedes Soares, C. 2005a. Impact characterisation of low fibre-volume glass reinforced polyester circular laminated plates. *International Journal of Impact Engineering* 31: 1-23.

Sutherland, L.S. & Guedes Soares, C. 2005b. Contact indentation of marine composites. *Composite Structures* 70(3): 287–94.

Sutherland, L.S. & Guedes Soares, C. 2006. Impact behaviour of typical marine composite laminates. *Composites Part B: Engineering* 37(2-3): 89-100.

Sutherland, L.S. & Guedes Soares, C. 2007. Scaling of impact on low fibre-volume glass-polyester laminates. *Composites Part A: Applied Science and Manufacturing* 38: 307-317.

Taylor, E.S. 1974. *Dimensional analysis for engineers.* Oxford: Clarendon Press.

Wisnom, M.R. 1999. Size effects in the testing of fibre-composite materials. *Composites Science and Technology* 59(13): 1937-1957.

Zhou, G. & Davies, G.A.O. 1995. Impact response of thick glass fibre reinforced polyester laminates. *International Journal of Impact Engineering* 16(3): 357-374.